3D MATERIALS SCIENCE

Microstructure-Sensitive Computational Estimates of Driving Forces for Surface Versus Subsurface Fatigue Crack Formation in Duplex Ti-6Al-4V and Al 7075-T6

KRZYSZTOF S. STOPKA [1,3] and DAVID L. MCDOWELL[1,2]

1.—Woodruff School of Mechanical Engineering, Georgia Institute of Technology, Atlanta, GA 30332, USA. 2.—School of Materials Science and Engineering, Georgia Institute of Technology, Atlanta, GA 30332, USA. 3.—e-mail: Kstopka3@gatech.edu

Statistical realizations of three-dimensional digital microstructures with different crystallographic orientation distributions, grain shapes, and grain size distributions are subjected to uniaxial cyclic straining to compare the cases of bulk and free surface on driving forces for fatigue crack formation. Crystal plasticity finite element simulations are conducted using both fully periodic (more representative of the bulk) and traction-free (i.e., free surface) boundary conditions for duplex Ti-6Al-4V and rolled Al 7075-T6. Following elastic–plastic shakedown, mesoscale volume-averaged fatigue indicator parameters (FIPs) are computed within fatigue damage process zones of grains and are fit to known extreme value distributions (EVDs). Owing to differences in crystallographic slip symmetry, FIPs for fcc Al 7075-T6 statistically occur much closer to the traction-free surface than for hcp Ti-6Al-4V. Additionally, surface versus bulk EVDs of FIPs vary differently for the two material systems, indicating a coupled role of microstructure and surface proximity that had not been previously elucidated.

INTRODUCTION

Understanding the physical mechanisms that govern fatigue behavior of polycrystalline duplex Ti-6Al-4V (Ti64) and Al 7075-T6 (Al7075) is crucial in naval aviation applications. Al7075 is a precipitation-hardened alloy used extensively in aerospace structural applications because of its high strength and low density. In applications that demand additional strength with cost as a secondary factor, Ti64 is used for its high-temperature strength, corrosion resistance, and high strength-to-weight ratio. Due to increased anisotropy of the hcp crystal structure, crystallographic effects dominate Ti64, whereas the increased symmetry of fcc Al7075 renders it more sensitive to grain morphology. As such, the mechanisms of fatigue crack formation and growth in the high cycle fatigue (HCF) regime differ for these alloys and depend on their microstructure attributes. The presence of a free surface exerts additional influence beyond that of bulk interactions, which may significantly affect driving forces for fatigue crack formation.[1,2] This effort builds on a previous study by Przybyla and McDowell,[3] in which driving forces for surface versus subsurface fatigue crack formation were examined for different Ti64 microstructures. Microstructure-sensitive crystal plasticity finite element method (CPFEM) models are used to assess the surface and bulk responses of these two alloys.

The effect of certain microstructure attributes on fatigue life is clear: a finer grain size leads to improved fatigue resistance due to shorter mean free paths for slip, and grain boundaries promote retardation of crack growth.[4] However, the effects of other key attributes (crystallographic texture, grain shape, and grain size distribution) are not obvious or intuitive, particularly regarding how neighboring grains/phases affect slip near the free surface. This work explores interactions between these key microstructure attributes, comparing the effects of bulk and free surface cases on driving forces for fatigue crack formation in Ti64 and Al7075.

Microstructure-Sensitive Computational Estimates of Driving Forces for Surface Versus
Subsurface Fatigue Crack Formation in Duplex Ti-6Al-4V and Al 7075-T6

29

METHODOLOGY

To examine the interactions among crystallographic texture, grain shape, and grain size variation and how they are affected by the presence of a free surface, different variants of Ti64 and Al7075 microstructures are instantiated with the open source Dream.3D[5] software. Statistical volume element (SVE) ensembles are subjected to fully reversed cyclic straining using CPFEM models specific to each alloy. Volume-averaged fatigue indicator parameters (FIPs) are calculated within damage process zones of each grain, with reference to specific slip systems. FIPs are used as surrogate measures for driving forces for fatigue crack formation. Due to the rare-event nature of fatigue, these FIPs are fit to known extreme value distributions (EVDs) to distinguish and rank order the minimum fatigue resistance of variant microstructures as a function of loading and boundary conditions. FIPs from the simulations with traction-free boundary conditions are located with respect to their distance from the SVE boundary to assess the relative influence of the free surface on fatigue crack formation compared with bulk microstructure.

Dream.3D Microstructure Generation

Dream.3D[5] is used to instantiate ensembles of SVEs for different microstructure variants of Ti64 and Al7075 for use with the CPFEM models. Typical CPFEM simulation outputs include fields of stress, strain, and inelastic strain, from which common macroscopic quantities of interest may be determined, such as elastic stiffness or yield strength. The size of the representative volume element (RVE) for these particular macroscopic quantities is relatively small compared with that for local responses such as maximum cyclic plastic strain and local driving forces such as FIPs for fatigue crack formation due to their rare-event nature.[6,7] Accordingly, ensembles of statistical samples (i.e., SVEs) are used to compute the statistical distribution of FIP responses.[8] Each SVE ensemble consists of 30 SVEs, and unique SVE instantiations are employed for both fully periodic (representative of bulk material response) and traction-free (i.e., free surface on one set of parallel faces) simulations. The latter condition is representative of a sheet of material with a relatively high surface area-to-volume ratio. It is therefore important to establish that the sheet thickness is large enough to capture near-bulk conditions at the center. SVE instantiations for both material systems are cubic with $(30)^3$ elements.

The Ti64 SVEs vary in both texture and grain size distribution, whereas composition is held constant at 50% α phase and 50% $\alpha + \beta$ colony phase. Ti64 textures are chosen based on previous work and literature, and they include β-annealed (determined by EBSD and achieved by annealing above the α–β transus temperature and cooling at an appropriate rate[9,10]), random (typical of powder metallurgy components), and basal-transverse and transverse (because of unidirectional rolling at 800°C and 960°C, respectively[11,12]). Orientation distribution function (ODF) pole figures are shown in Fig. 1. The lognormal grain size is set to 60 ± 15 μm for simulations comparing the effects of different textures and straining directions, whereas simulations aimed at comparing the effects of grain size distributions employ an average lognormal grain size of 60 μm with standard deviations of 10 μm, 20 μm, and 30 μm using the random and transverse textures. These two textures are chosen to study the effects of grain size distribution because they represent the extremes of the Ti64 textures simulated. Regarding the effects of grain size distribution, the random texture is uniaxially strained only in the X direction, whereas the transverse texture is uniaxially strained in the X and Z directions [left–right and into-out of the page direction relative to the $\langle 0001 \rangle$ (leftmost) pole figure in Fig. 1d, respectively; this convention is retained throughout this work]. The cubic SVE volume is set to $(300$ μm$)^3$, with an average of 264 grains per SVE. In addition to ODFs, Dream. 3D also incorporates misorientation distribution functions to consider target grain disorientation distributions.

Three textures of Al7075 are chosen, which include cubic (observed after recrystallization or homogenization heat treatment[13]), random, and rolled (observed after cold rolling[14]); ODF pole figures are shown in Fig. 1. The lognormal grain size is set to 14 ± 2 μm for simulations comparing the effects of different textures and grain elongation. An average lognormal grain size of 14 μm with standard deviations of 2 μm, 4 μm and 6 μm is used to study the effects of grain size distributions for the three Al7075 textures with equiaxed grains. Zhao and Jiang[15] found the Al7075 grain elongation ratio after cold working to be as severe as 7:1:1, and so a range of grain elongation ratios was chosen to study their effect on fatigue response, which includes 1:1:1 (equiaxed), 3:1:1, 5:1:1, and the experimentally observed 7:1:1. The cubic SVE volume is set to $(75$ μm$)^3$, with an average of 278 grains per SVE.

Crystal Plasticity Finite Element Method Models

The microstructure-sensitive CPFEM models employ a multiplicative decomposition of the deformation gradient, a rate-sensitive power law slip system flow rule, and associated hardening rules.[16–18] The models are implemented as User MATerial (UMAT) subroutines into the ABAQUS[19] finite element package. Hennessey et al.[16] investigated various constitutive models for the mechanical modeling of Al7075, specifically considering different back stress formulations for the crystal plasticity. The model was calibrated to match experimental stress–strain data, including
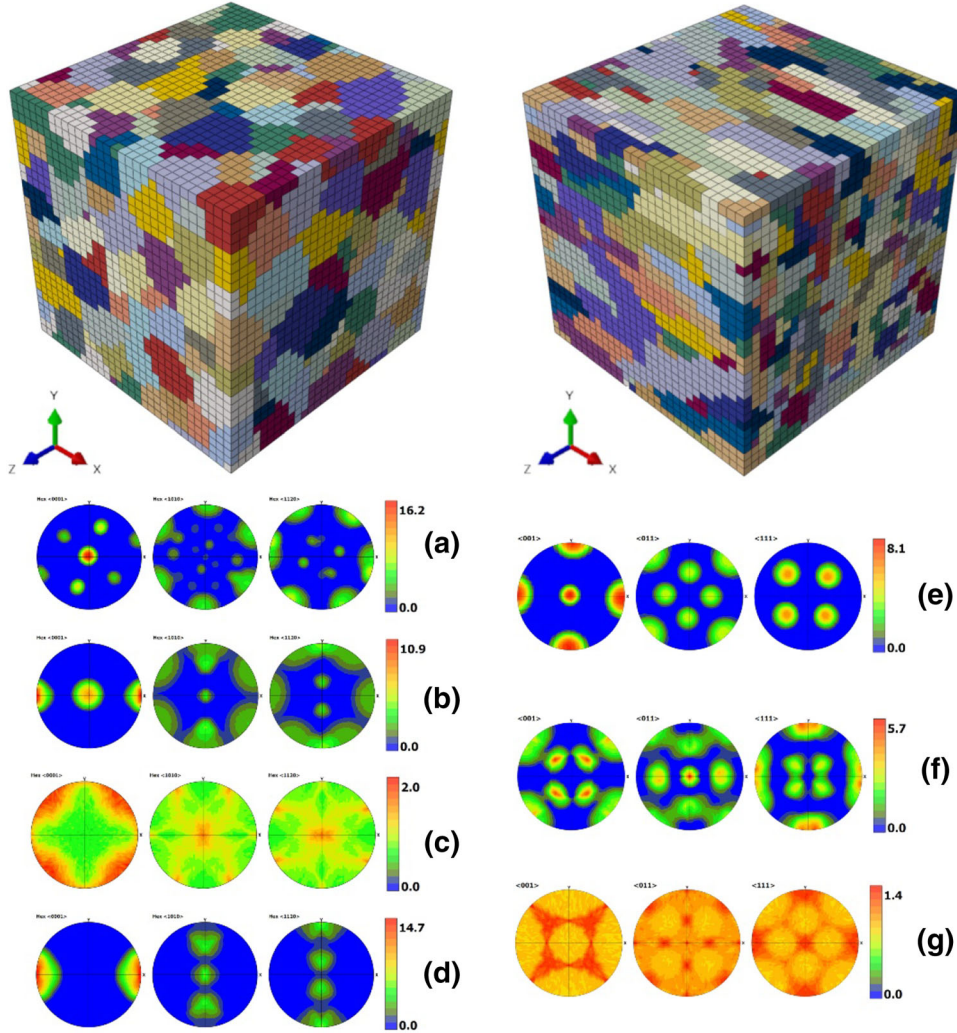
Fig. 1. Sample SVE instantiations for equiaxed Ti-6Al-4V (top left) and rolled Al 7075-T6 (7:1:1 grain elongation ratio) (top right). From left to right: $\langle 0001 \rangle$, $\langle 10\overline{1}0 \rangle$ and $\langle 1\overline{2}10 \rangle$ ODF pole figures for Ti-6Al-4V textures: (a) β-annealed, (b) basal-transverse, (c) random, and (d) transverse. $\langle 001 \rangle$, $\langle 011 \rangle$ and $\langle 111 \rangle$ ODF pole figures for Al 7075-T6: (e) cubic, (f) rolled, and (g) random.

asymmetric strain-controlled cycling and mean stress relaxation behavior. The initial Ti64 crystal plasticity model, which accounted for three-dimensional slip system geometry and microstructure variation such as dislocation structure and crystallographic texture, was developed by Mayeur and McDowell.[17] Although Ti64 colony grains consist of alternating laths of secondary α and β phases, they are homogenized because of computational constraints.[17] Zhang et al.[18] expanded the constitutive model to capture length scale effects associated with dislocation interactions between various microstructure features for both monotonic and cyclic loading. Smith et al.[10] calibrated elastic constants, critical resolved shear stress (CRSS) values, and other power law flow rule parameters. One of the limitations of these models is that slip transfer between grains/phases is not explicitly considered, whether within α–β colonies or at α–α or primary α boundaries with colonies; these interfaces are treated as impenetrable to slip in this

present model. Hence, detailed digital rendering of grain/phase boundaries is not warranted in the present work.

Loading Parameters

Simulation parameters are held constant for both alloys. Three fully reversed ($R_\varepsilon = -1$) uniaxial straining cycles are applied at a strain rate of 0.001 s^{-1} to a maximum strain of 0.8% (corresponding to HCF conditions, in which loading at the macroscale is below the polycrystal yield point of the materials considered), with zero initial strain and zero initial back stress, to promote elastic–plastic shakedown. Preliminary analysis has shown that volume-averaged FIPs vary by < 1% after additional straining cycles, and so three cycles suffice for elastic–plastic shakedown (and FIP saturation). Loading is quasi-static, and the strain rate is used to determine the time step for the simulations. Temperature is assigned as 300 K and straining is

initiated in compression. The traction-free surfaces for Al7075 are normal to the Z-axis, so that the free surface is representative of the normal direction relative to the rolling process, while straining is performed in the X-axis, representative of the rolling direction. The traction-free surfaces for Ti64 are set normal to the Y-axis, and uniaxial straining is performed in the X- and Z-axis. These straining directions are studied in Ti64 because the strong anisotropy of the hcp crystal structure is expected to cause pronounced effects of load orientation.

Fatigue Indicator Parameters

The use of FIPs as surrogate measures for the driving force to form fatigue cracks has been extensively documented.[8,20,21] Fatemi and Socie[22] proposed a critical plane-based FIP, defined as

$$\text{FIP}_{\text{FS}} = \frac{\Delta\gamma_p^{\max}}{2}\left[1 + k\,\frac{\sigma_n^{\max}}{\sigma_y}\right] \qquad (1)$$

where $\Delta\gamma_p^{\max}$ is the maximum cyclic plastic shear strain range, $\sigma_n^{\max}$ is the peak stress normal to the slip plane of $\Delta\gamma_p^{\max}$, σ_y is the macroscopic yield strength of the material, and k is a constant that controls the influence of the normal stress; k is typically between 0.5 and 1. McDowell and Berard[23] showed that FIP_{FS} can be used to correlate the rate of microcrack propagation by analogy to the ΔJ-integral of elastic–plastic fracture mechanics. Several types of FIPs can be defined,[20] which may aim to model crack formation along slip bands within individual grains or crack formation along grain boundaries because of the accumulation of net plastic strain, which leads to intergranular fatigue crack formation and growth. Other fatigue parameters include measures of local stored energy density.[24]

Castelluccio and McDowell[25] reported close correlation between a crystallographic version of the Fatemi–Socie FIP (FIP_α) and the cyclic crack tip displacement range (ΔCTD) for cracks lying along the interface of slip bands and matrix in a single crystal and in homogeneous single crystals. This allows for the use of a relatively coarse mesh to compute FIP_α, whereas measurements of ΔCTD would require highly refined elements, which would be computationally prohibitive. Consequently, FIP_α serves as a surrogate measure of fatigue crack formation driving force within individual grains and is defined as

$$\text{FIP}_\alpha = \frac{\Delta\gamma_p^\alpha}{2}\left[1 + k\,\frac{\sigma_n^\alpha}{\sigma_y}\right] \qquad (2)$$

where $\Delta\gamma_p^\alpha$ is the range of cyclic plastic shear strain on slip system α without ratcheting,[21] with the peak stress normal to this slip plane defined as σ_n^α. Here, k and σ_y retain their meaning from Eq. 1. While

FIP_{FS} is calculated using the stress and plastic strain tensors at each element, FIP_α is calculated using quantities specific to each slip system. In this work, FIP_α values are computed based on $\Delta\gamma_p^\alpha$ and σ_n^α calculated during the final straining cycles with $k = 1$ for Ti64 and $k = 10$ for Al7075 (this higher value of k was previously determined to correlate better between various loading conditions of Al7075 to experimental fatigue lives[26]). The effect of the parameter k on the fatigue rank ordering of Al7075 is examined later. Hereafter, we will focus on FIP_α and refer to it simply as FIP.

FIPs are computed for each element integration point in the discretized microstructures and must be appropriately volume averaged, since fatigue crack formation occurs over some finite damage process zone. This also alleviates mesh sensitivity via regularization.[25,27] The averaging volume is held fixed across different simulations so that appropriate comparison can be made between different textures, grain morphologies, and loading conditions. Although FIPs may be averaged over entire grains, this smears out extreme values of individual element FIPs. Additionally, different grain size distributions will lead to different averaging volumes. Castelluccio and McDowell[27,28] introduced the concept of grain "banding," in which the digital grains of SVEs are split into bands representative of the material's crystallographic slip planes to be used as the volume-averaging domains (see Fig. 2a). Band width is usually maintained at one or two elements. This reduces the FIP averaging domain to regions within the grain, but results in bands of significantly varying volumes. In this work, each grain is banded as proposed by Castelluccio and McDowell, but the bands are then further divided into sub-band regions (see Fig. 2b). Each band is analyzed so that combinations of a selected number of adjacent elements (in this work, eight) may be identified and designated as unique sub-band regions. Volume averaging then takes places over these regions, providing a regularized volume-averaging scheme and an associated non-local FIP.

The 12 octahedral slip systems of the fcc crystal structure have identical initial resistance to slip and consist of four slip planes, each with three slip directions. Grains of fcc Al7075 are banded along these four planes, as shown in Fig. 2a. In contrast, the low symmetry of the Ti64 hcp crystal structure results in slip systems with different CRSS values; slip activity is dominated by the basal and prismatic slip systems because of their relatively lower CRSS values.[10,18] Because the pyramidal slip systems in Ti64 are more difficult to activate, their slip planes are not included in the banding process to compute associated FIPs. Ti64 grains are banded along the single basal and three prismatic slip planes; experimental findings show that fatigue crack formation and growth in Ti64 occur predominantly on these slip systems.[29,30]
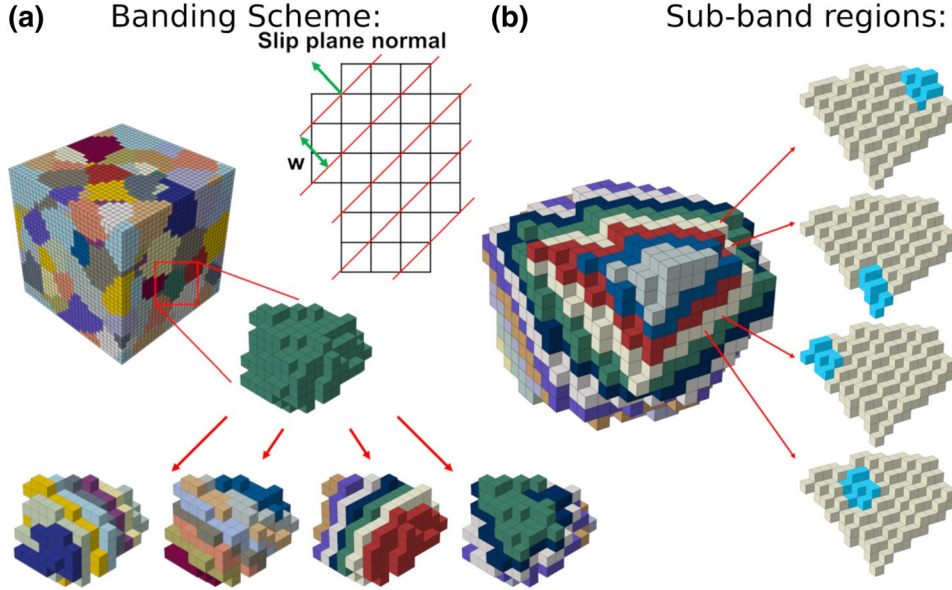
Fig. 2. (a) Banding scheme for an SVE with equiaxed grains that depicts a single grain banded along four different slip planes. (b) Four unique sub-band regions in the white band are highlighted.

Extreme Value Statistics

For each SVE ensemble, the single highest sub-band averaged FIP of each grain is identified. These FIPs are compiled and fit to the Gumbel (type I) EVD,[3,31–33] defined as

$$F_{Y_n}(y_n) = \exp\left[-e^{-\alpha_n(y_n - u_n)}\right] \quad (3)$$

where $F_{Y_n}(y_n)$ is the probability that the value Y_n will be $\leq y_n$, u_n is the characteristic largest value of the sampled population, and α_n is an inverse measure of dispersion of the largest value of the population. Although each compiled list contains nearly 8100 FIPs (~ 270 grains per SVE for 30 SVEs), the highest 50 are chosen because they are expected to be most detrimental to fatigue resistance. These highest 50 FIPs from each ensemble are sorted in ascending order, and their probability is estimated by

$$F_{Y_j}(y_j) = \frac{j - 0.3}{n + 0.4} \quad (4)$$

where n is the number of FIPs examined and j is the rank order of the corresponding FIP. For plotting and regression purposes, the Gumbel distribution is rewritten as a linear function of y in the form of

$$\ln\left[\ln\left(\frac{1}{F_{Y_n}(y_n)}\right)\right]^{-1} = \alpha_n y_n - \alpha_n u_n \quad (5)$$

in which α_n is the slope and $-\alpha_n u_n$ is the y-intercept. In this linearized form, a true extreme value Gumbel distribution appears as a straight line. FIPs from different ensembles fit to this linearized form of the Gumbel distribution then facilitate the rank ordering of fatigue resistance between different microstructure variants.

RESULTS

To quantify possible effects of the traction-free surface on cyclic slip intensity, the relative difference between stress and plastic strain is computed for 30 Ti64 and Al7075 SVEs representing the same microstructures with random crystallographic texture, i.e., 30 SVEs are subjected to uniaxial cyclic straining with both fully periodic and traction-free boundary conditions.[3] Stress and plastic strain is then averaged across planes one element thick, oriented normal to the traction-free boundaries, and compared between the two sets of simulations. The relative difference of the stress component in the direction of applied straining σ_{11} and effective plastic strain (i.e., $\varepsilon_{\mathrm{eff}} = \sqrt{(2/3)\varepsilon^p : \varepsilon^p}$ where ε^p is the plastic strain tensor) is defined as

$$E_r = \frac{|x_f - x_p|}{x_f}, \quad (6)$$

where x_f and x_p represent either the stress or plastic strain defined above for traction-free and fully periodic boundary conditions, respectively. The maximum relative difference at the free surface for σ_{11} and $\varepsilon_{\mathrm{eff}}$ reaches 0.78% and 22.0% and is as low as 0.05% and 1.3% in the center of the SVE, respectively, for Ti64. While there appears to be some influence of the free surface at the center of the SVEs, this effect is minimal and compares favorably with previous work,[3] in which the relative difference of the effective plastic strain remained as high as 13% at the center of the SVEs. For Al7075, the maximum relative difference at the free surface for σ_{11} and $\varepsilon_{\mathrm{eff}}$ reaches 8.0% and 15.3% and is as low as 6.7% and 6.9% in the center of the SVE, respectively. The high symmetry of the fcc Al7075

Microstructure-Sensitive Computational Estimates of Driving Forces for Surface Versus Subsurface Fatigue Crack Formation in Duplex Ti-6Al-4V and Al 7075-T6
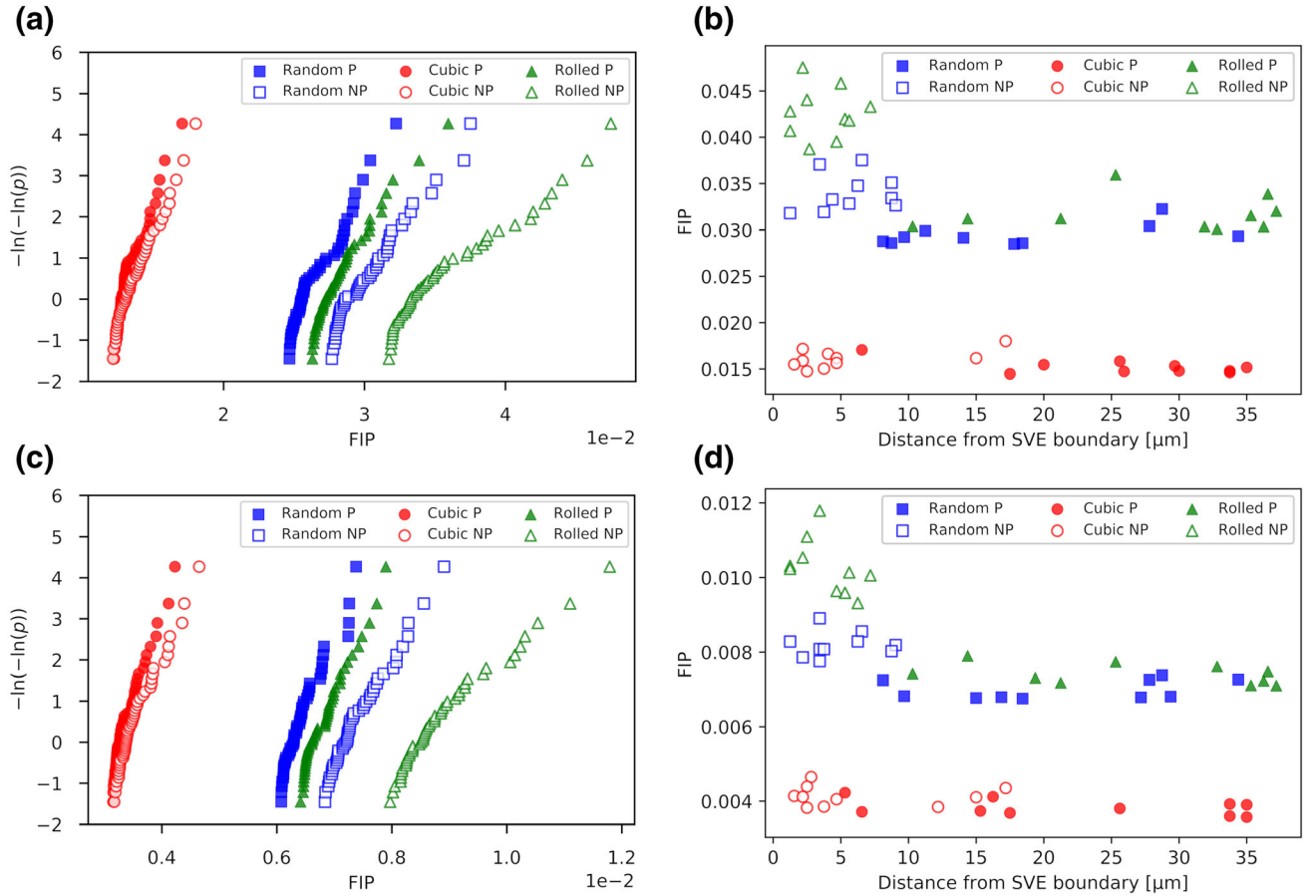
33

Fig. 3. Gumbel EVD of the highest 50 Al 7075-T6 FIPs (equiaxed grains) with varying texture for surface (NP) and bulk (P) boundary conditions using (a) $k = 10$ and (c) $k = 1$ in Eq. 2. Location of the ten highest FIPs using (b) $k = 10$ and (d) $k = 1$ in Eq. 2 with respect to the free surface (i.e., SVE boundary).

crystal structure results in stronger interactions between the microstructure and free surface compared with Ti64. This suggests that further studies with larger thicknesses might be pursued for Al7075, thereby allowing for an improved consideration of the change of constraint from the free surface to the bulk of the material.

Figure 3a and c presents the highest 50 non-local, sub-band averaged FIPs (hereby referred to simply as FIPs) compiled from distinct grains for surface and bulk simulation SVE ensembles of equiaxed Al7075 that vary solely in texture for $k = 10$ and $k = 1$, respectively. The parameter k (which controls the influence of the normal stress component in Eq. 2) affects the resulting FIP magnitudes, but not the rank ordering of the FIPs. The differences in FIP magnitudes and importance of the parameter k are critical when using FIPs to determine crack growth rates or absolute fatigue lives, as was done by Castelluccio and McDowell.[28,34] However, this work solely considers the relative rank ordering of different types of microstructures.

The cubic and rolled textures exhibit the lowest and highest FIPs, respectively, indicating the rolled texture's higher propensity to form fatigue cracks

(for the specific case of uniaxial straining in the rolled direction). The random texture exhibits moderate FIPs. Free surface effects intensify FIP response; traction-free boundary conditions increase FIPs significantly for the random and rolled textures, but only slightly for the cubic texture. Additionally, cubic textured FIPs at low cumulative probabilities tend to merge, whereas they remain separate at all probabilities for the random and rolled textures. The ten highest FIPs from each SVE ensemble are plotted as a function of their distance from the SVE boundary (i.e., the centroid of the eight-element sub-band region over which the FIPs are averaged) to examine possible interactions between the free surface and crystallographic texture (shown in Fig. 3b and d). FIPs from the fully periodic simulations (with labels "P") and their locations are included to show their tendency to form throughout the SVE, whereas the traction-free surface FIPs (with labels "NP") have a much stronger propensity to lie closer to the free surface.

Elongation of grains in Al7075 due to rolling may have significant effects on fatigue behavior.[15] Figure 4a and b presents the highest 50 FIPs compiled from unique grains for surface and bulk simulation
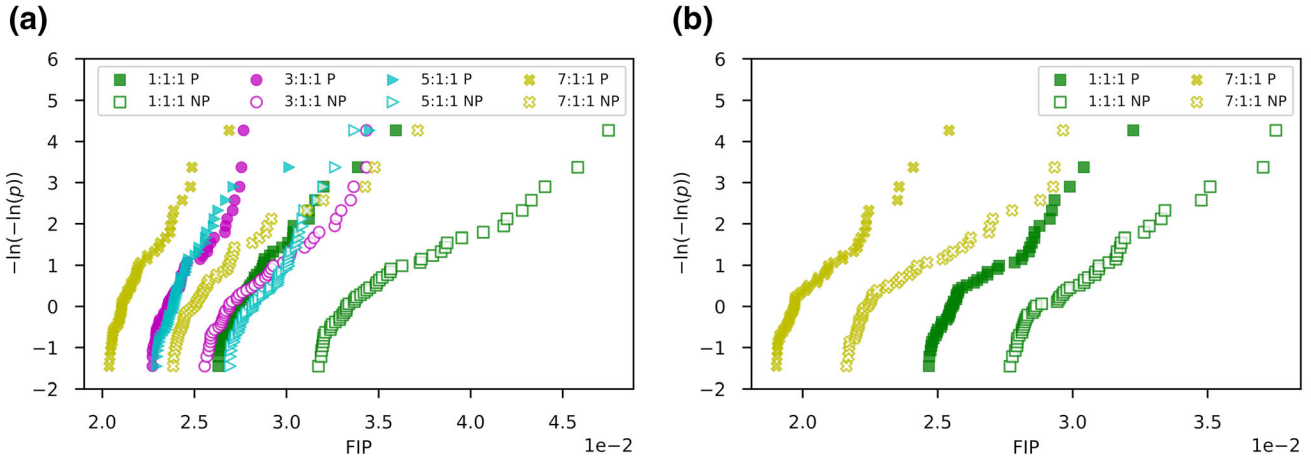
(a)

(b)

Fig. 4. Gumbel EVD of the highest 50 Al 7075-T6 FIPs for (a) rolled and (b) random texture with varying grain elongation for surface (NP) and bulk (P) boundary conditions.
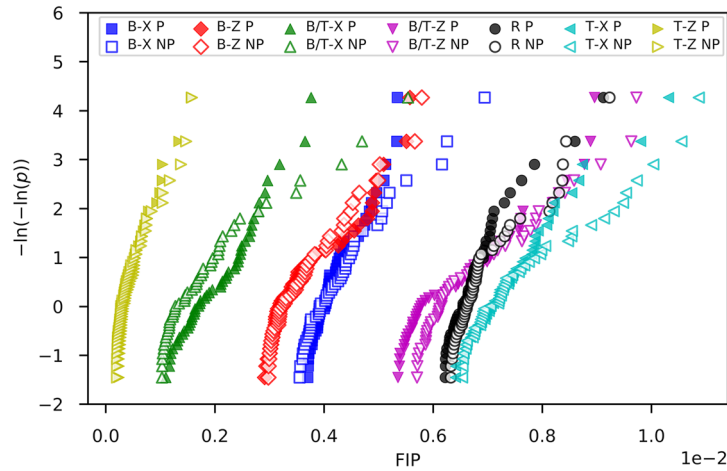

Fig. 5. Gumbel EVD of the highest 50 Ti-6Al-4V FIPs with varying texture (β-annealed, B; basal-transverse, B/T; random, R; transverse, T) and straining direction (X or Z directions relative to $\langle 0001 \rangle$ ODF pole figure in Fig. 1) for surface (NP) and bulk (P) boundary conditions.

SVE ensembles of Al7075 with rolled and random texture, respectively, and varying grain elongation. FIPs for equiaxed grains (grain elongation ratio of 1:1:1) are the highest in magnitude and steadily decrease, with the most severe elongation (7:1:1) exhibiting the lowest FIPs. The random texture is simulated with only equiaxed and 7:1:1 grain elongation ensembles to verify that the observed effects are due to grain morphology and are independent of texture. Recall that uniaxial straining is applied in the direction of the elongated grains. The potency of this morphologic effect rivals crystallographic texture effects for this alloy system. SVEs and grains with different grain elongation ratios maintain a constant number of grains and consistent grain volume statistics, respectively; this additional analysis is shown in Tables S-1, S-2 and Fig. S-1 (refer to online supplementary material). Therefore, an equivalent number of grains is sampled for all elongation ratios.

Ti64 SVE ensembles are subjected to uniaxial cyclic straining in both the X and Z directions to examine the combined effects of a free surface, crystallographic texture, and uniaxial straining direction. The highest 50 FIPs for the four Ti64 textures strained in the two directions are shown in Fig. 5. The random texture is loaded only in the X direction, because no difference is expected in the FIP response between different straining directions. In contrast to Al7075, there is only a slight increase in FIP magnitude between surface and bulk loading conditions; the transverse texture strained in the Z direction (T-Z) shows little, if any, increase. This same texture strained in the X direction (T-X), however, results in the highest FIPs observed and correlates with experimental findings by Peters et al.,[11] who found that this combination of texture and loading direction resulted in the lowest fatigue strength out of the five they considered. This same experimental study, however, did not exhibit the

superior performance of the T-Z texture shown here, which may indicate that FIPs below a certain threshold may not serve as adequate surrogate measures for fatigue crack formation driving force (many of the T-Z FIPs are close to zero). Conversely, the β-annealed texture exhibits little difference regarding the straining direction, whereas the basal-transverse texture shows intermediate sensitivity. Although the Transverse texture strained in the Z direction manifests the lowest FIPs, other factors must be considered in the process of material selection and component design. This texture's high sensitivity to straining direction may create issues for the fatigue design of components if not accounted for. Additionally, performance requirements such as elastic stiffness and yield strength must be considered; the transverse texture loaded in the Z direction exhibits the lowest stiffness and
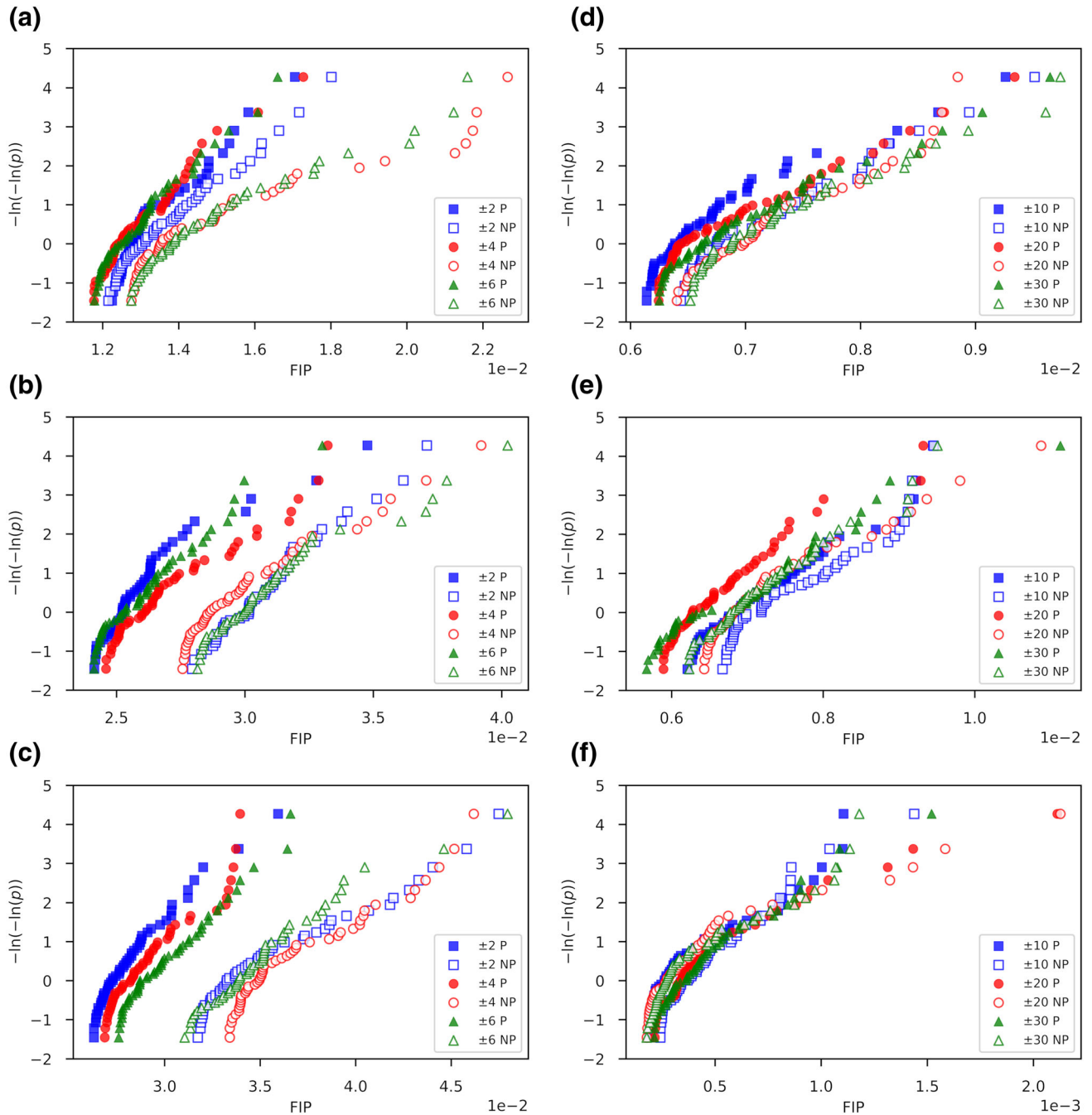

Fig. 6. Gumbel EVD with varying grain size variation for the highest 50 Al 7075-T6 FIPs of (a) cubic, (b) random, and (c) rolled texture and the highest 50 Ti-6Al-4V FIPs of (d) random, (e) T-X, and (f) T-Z texture for surface (NP) and bulk (P) boundary conditions. All grains are equiaxed.
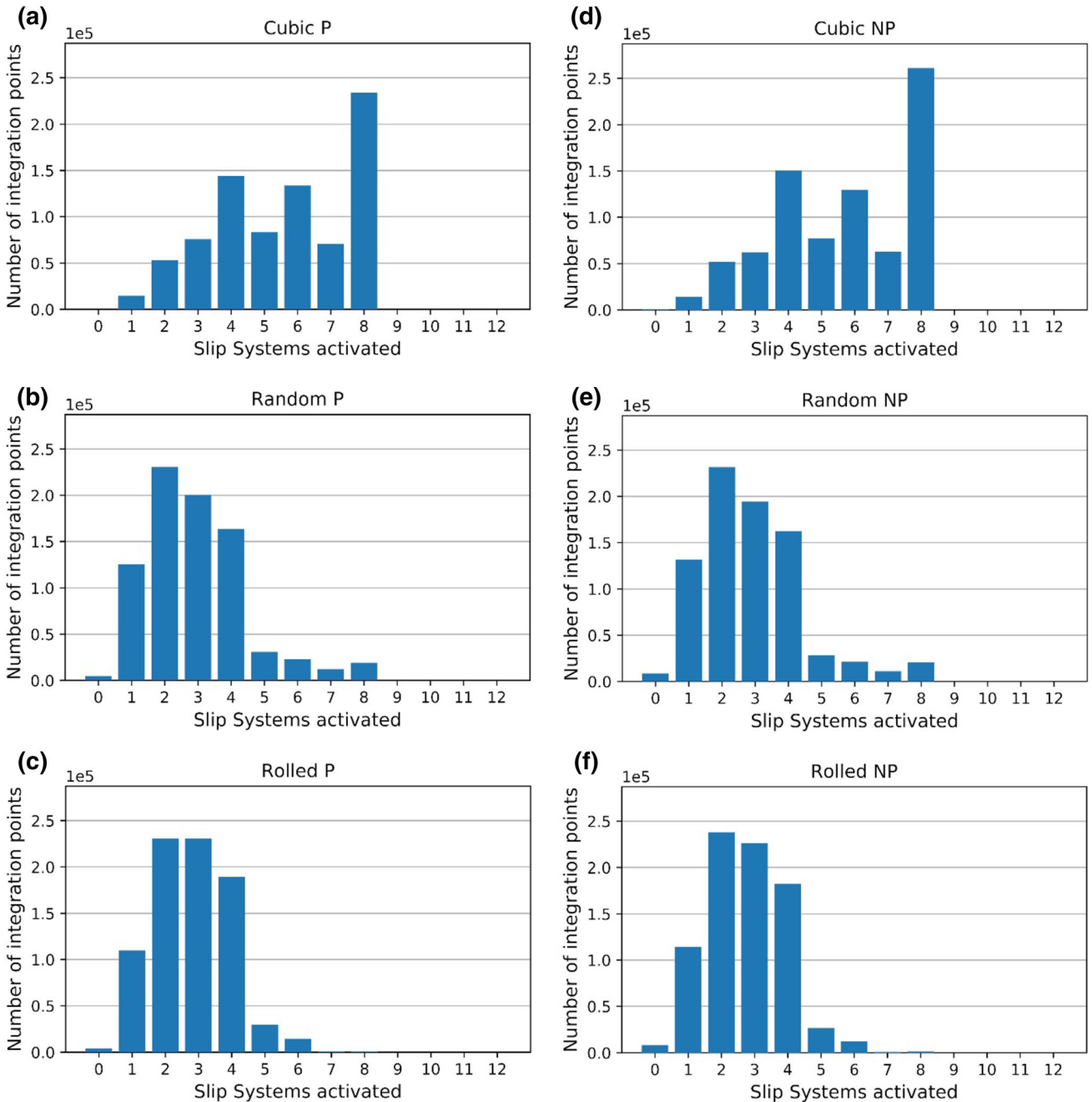
Fig. 7. Number of integration points with a select number of slip systems active (criteria: plastic shear strange range > 0.00001) for (a, d) cubic, (b, e) random, and (c, f) rolled texture of equiaxed Al 7075-T6 for surface (NP) and bulk (P) simulations. Crystallographic slip is more homogeneously distributed in the cubic texture compared with the random and rolled textures.

strength.[11] To ensure enough grains are sampled during FIP compilation, Al7075 and Ti64 FIPs are fit to the Gumbel EVD using 10 SVEs, 20 SVEs, and 30 SVEs per ensemble. While minor differences are observed when comparing EVDs of FIPs from 10 SVEs and 20 SVEs per ensemble, there is little difference in FIP position and no difference in the rank ordering observed in the figures when comparing EVDs of FIPs from 20 SVEs and 30 SVEs per ensemble. Therefore, we conclude that ensembles of 30 SVEs are sufficient for the rank ordering of

textures, grain morphologies, and straining directions (with the specified number of grains per SVE used in this study). However, the different number of slip systems in these two materials may affect this number, as well as the fact that Ti64 contains two phases, which may affect the total volume occupied by the most detrimental phase regarding fatigue resistance.

The effects of grain size variation in Al7075 for the cubic, random, and rolled texture are shown in Fig. 6a–c, respectively. The intent of these

simulations is to determine how grain nearest neighbors affect FIP response; a wider grain size variation will increase the probability that the FIP value for a grain will be influenced by an increased number of neighboring grains. The cubic textured FIPs in Fig. 6a vary at high cumulative probabilities but tend to merge at low to mid cumulative probabilities; an increase in grain size variation for traction-free conditions significantly increases FIP magnitude. In contrast, the FIPs for the traction-free random texture (Fig. 6b) display a uniform increase in FIP magnitude at all cumulative probabilities. Lastly, the rolled texture (Fig. 6c) displays a similar uniform increase in magnitude, which is exacerbated at the highest cumulative probabilities. The rank ordering of FIP magnitudes as a function of grain size variation is non-intuitive and changes for each texture, indicating non-trivial interactions among the texture, grain size variation, and influence of a free surface in Al7075.

Less extreme effects of grain size variation are observed for Ti64. Little effect of the free surface is observed in comparing the random and T-X simulations (Fig. 6d and e, respectively), but the rank ordering of FIP magnitudes is flipped: the largest grain size variation in random textured SVEs results in FIPs of the highest magnitude, whereas they are the lowest for T-X. FIPs calculated for the T-Z straining condition (Fig. 6f) only vary at the highest cumulative probabilities and merge at low cumulative probabilities, as the FIPs quickly tend to zero. The non-trivial effects observed for Al7075 hold true for Ti64 and may require advanced probabilistic frameworks (such as use of extreme value marked correlation functions) for further elucidation.[32,33]

DISCUSSION

FIPs are further examined by considering their surface proximity in the traction-free simulations. The average distance from the traction-free boundary of the ten highest Al7075 FIPs from ensembles varying in texture with equiaxed grains (Fig. 3a) and grain elongation with rolled grains (Fig. 4a) is computed. The minimum and maximum average distances are 3.77 μm and 9.19 μm, respectively, indicating a strong propensity for these FIPs to occur near the surface. If the FIPs had no propensity to occur near the free surface, the average values would be around 18.75 μm (half of 37.5 μm, which is the maximum distance from the free surface to the center of the Al7075 SVEs). FIPs with rolled texture and equiaxed grains are the highest in magnitude, with the lowest average distance to the free surface (3.77 μm). However, this rank ordering between FIP magnitude and average distance to the free surface does not hold true for the remaining FIPs. There may be a

threshold on Al7075 FIPs above which the propensity to occur very close to the free surface is strongest.

For Ti64, the minimum and maximum average distances are 29.9 μm and 73.4 μm, respectively. Since the Ti64 SVEs are larger, an average distance from the surface of 75 μm would indicate negligible preference for the highest FIPs to occur near the traction-free boundary (half of 150 μm, which is the maximum distance from the free surface to the center of the Ti64 SVEs). Therefore, the Ti64 FIPs have a much weaker propensity to occur near the free surface compared with Al7075 FIPs. This suggests that the increased crystallographic slip and elastic symmetry of fcc Al7075 result in stronger interactions between individual grains and the free surface. In contrast, the low symmetry of hcp Ti64 appears to result in much stronger interactions between neighboring grains, which dominates free surface effects. Additionally, the Ti64 SVEs are multiphase (50% α phase and 50% $\alpha + \beta$ colony phase), whereas Al7075 is single phase. Rank ordering between FIP magnitude and average distance from the free surface mimics that of Al7075, except for the β-annealed texture loaded in the Z direction; FIPs of higher magnitude appear to occur closer to the free surface, whereas the lowest FIPs tend to occur throughout the SVE.

Ti64 FIPs vary mainly at high cumulative probabilities and tend to merge at mid to low cumulative probabilities (in the majority of textures and straining directions considered). In contrast, Al7075 FIPs display clear separation at all cumulative probabilities (excluding the cubic texture, which varies the least between free surface and bulk boundary conditions). To investigate these EVD FIP tendencies, the number of activated slip systems in different Al7075 textures is analyzed.

For the three Al7075 textures with equiaxed grains, the plastic shear strain range during the last loading cycle is extracted for each integration point and for each of the 12 slip systems. Figure 7 shows the number of integration points with a select number of slip systems active (defined as having a plastic shear strain range > 0.00001). While there is a minor difference between surface and bulk slip system activation, slip activity is more homogeneously distributed in the cubic texture (Fig. 7a and d), with the greatest number of integration points having eight active slip systems; four, six, and eight active slip systems are most prevalent.

CONCLUSION

This work explores differences in EVDs of driving forces for fatigue crack formation in Al7075 and Ti64 for a range of microstructure variants for several uniaxial cyclic straining directions, comparing cases representative of bulk and free surface. We find that:

- Different combinations of textures, straining directions, and surface versus bulk boundary conditions for the two alloys result in different rank ordering of fatigue resistance as reflected by EVDs of FIPs.
- Due to differences in crystal structure and symmetry, the fcc Al7075 grains interact much more strongly with the free surface in producing high FIP values than is observed for hcp Ti64, in which individual grain/phase interactions dominate and no preference is indicated for surface-correlated activity.
- FIPs of the highest magnitude have a strong propensity to occur much closer to the free surface for Al7075 than for Ti64.
- For uniaxial cyclic straining along the rolling direction, an increase in grain elongation in Al7075 results in a corresponding reduction of FIP magnitudes.
- More homogeneous slip system activation may alleviate both FIP magnitude and the effect of a free surface in Al7075, as observed with the cubic texture.

This computational study points to a clear role for in situ 3D or 4D experimental studies to further focus on quantitative correlations of microstructure with proximity to the free surface in producing extreme values of lattice distortion and cyclic plastic deformation in fatigue. In particular, the new finding of this study of apparent fundamental and non-intuitive differences in this regard between the propensity for a high symmetry fcc Al alloy and a low symmetry hcp Ti alloy to promote elevated driving forces for fatigue crack formation near the free surface should be explored experimentally.

ACKNOWLEDGEMENTS

ELECTRONIC SUPPLEMENTARY MATERIAL

The online version of this article (https://doi.org/10.1007/s11837-019-03804-1) contains supplementary material, which is available to authorized users.

REFERENCES

1. I. Marines, X. Bin, and C. Bathias, *Int. J. Fatigue* 25, 1101 (2003).
2. K.S. Ravi Chandran and S.K. Jha, *Acta Mater.* 53, 1867 (2005).
3. C.P. Przybyla and D.L. McDowell, *Acta Mater.* 60, 293 (2012).
4. P.S. De, R.S. Mishra, and C.B. Smith, *Scr. Mater.* 60, 500 (2009).
5. M.A. Groeber and M.A. Jackson, *Integr. Mater. Manuf. Innov.* 3, 1 (2014).
6. D.L. McDowell, *Int. J. Damage Mech* 8, 376 (1999).
7. T. Kanit, S. Forest, I. Galliet, V. Mounoury, and D. Jeulin, *Int. J. Solids Struct.* 40, 3647 (2003).
8. D.L. McDowell and F.P.E. Dunne, *Int. J. Fatigue* 32, 1521 (2010).
9. B.D. Smith, D.S. Shih, and D.L. McDowell, *Int. J. Fatigue* 92, 116 (2016).
10. B.D. Smith, D.S. Shih, and D.L. McDowell, *Int. J. Plast* 101, 1 (2018).
11. M. Peters, A. Gysler, and G. Lütjering, *Metall. Mater. Trans. A* 15, 1597 (1984).
12. G. Lütjering, *Mater. Sci. Eng., A* 243, 32 (1998).
13. F.J. Humphreys and M. Hatherly, *Recrystallization and Related Annealing Phenomena*, 2nd ed., ed. F.J. Humphreys and M. Hatherly (Oxford: Elsevier, 2004), pp. 215–217.
14. P. Ramesh Narayanan, S. Suwas, K. Sreekumar, P.P. Sinha, and S. Ranganathan, *Mater. Sci. Forum* 702–703, 315 (2012).
15. T. Zhao and Y. Jiang, *Int. J. Fatigue* 30, 834 (2008).
16. C. Hennessey, G.M. Castelluccio, and D.L. McDowell, *Mater. Sci. Eng., A* 687, 241 (2017).
17. J.R. Mayeur and D.L. McDowell, *Int. J. Plast* 23, 1457 (2007).
18. M. Zhang, J. Zhang, and D.L. McDowell, *Int. J. Plast* 23, 1328 (2007).
19. Simulia, *ABAQUS* (Providence, RI: Dassault Systemes, 2007).
20. C.P. Przybyla, W.D. Musinski, G.M. Castelluccio, and D.L. McDowell, *Int. J. Fatigue* 57, 9 (2013).
21. D.L. McDowell, *Mater. Sci. Eng., A* 468–470, 4 (2007).
22. A. Fatemi and D.F. Socie, *Fatigue Fract. Eng. Mater. Struct.* 11, 149 (1988).
23. D.L. McDowell and J.-Y. Berard, *Fatigue Fract. Eng. Mater. Struct.* 15, 719 (1992).
24. B. Chen, J. Jiang, and F.P.E. Dunne, *Int. J. Plast* 101, 213 (2018).
25. G.M. Castelluccio and D.L. McDowell, *Int. J. Fract.* 176, 49 (2012).
26. C.D. Hennessey, *Masters Thesis* (George W. Woodruff School of Mechanical Engineering, Georgia Institute of Technology, 2015).
27. G.M. Castelluccio and D.L. McDowell, *Mater. Sci. Eng., A* 639, 626 (2015).
28. G.M. Castelluccio and D.L. McDowell, *Mater. Sci. Eng., A* 598, 34 (2014).
29. I. Bantounas, D. Dye, and T.C. Lindley, *Acta Mater.* 57, 3584 (2009).
30. F. Bridier, P. Villechaise, and J. Mendez, *Acta Mater.* 56, 3951 (2008).
31. E.J. Gumbel, *Statistics of Extremes* (New York: Dover Publications, 2004).
32. C.P. Przybyla and D.L. McDowell, *Int. J. Plast* 26, 372 (2010).
33. C.P. Przybyla and D.L. McDowell, *Int. J. Plast* 27, 1871 (2011).
34. G.M. Castelluccio and D.L. McDowell, *Int. J. Fatigue* 82, 521 (2016).

Publisher's Note Springer Nature remains neutral with regard to jurisdictional claims in published maps and institutional affiliations.